The electronic structure of organic-inorganic hybrid compounds

Zolfaghari, P.; de Wijs, G. A.; de Groot, R. A.

Published in:
Journal of Physics-Condensed Matter

DOI:
10.1088/0953-8984/25/29/295502

Publication date:
2013

IOP Publishing Journal of Physics: Condensed Matter
J. Phys.: Condens. Matter **25** (2013) 295502 (10pp) doi:10.1088/0953-8984/25/29/295502

The electronic structure of organic–inorganic hybrid compounds: $(NH_4)_2CuCl_4$, $(CH_3NH_3)_2CuCl_4$ and $(C_2H_5NH_3)_2CuCl_4$

P Zolfaghari[1], G A de Wijs[1] and R A de Groot[1,2]

[1] Institute for Molecules and Materials, Radboud University Nijmegen, Heyendaalseweg 135, 6525 AJ Nijmegen, The Netherlands
[2] Solid State Materials for Electronics, Zernike Institute for Advanced Materials, University of Groningen, Nijenborgh 4, 9747 AG Groningen, The Netherlands

E-mail: zolfaghari@science.ru.nl and r.degroot@science.ru.nl

Received 1 May 2013
Published 27 June 2013
Online at stacks.iop.org/JPhysCM/25/295502

Abstract
Hybrid organic–inorganic compounds are an intriguing class of materials that have been experimentally studied over the past few years because of a potential broad range of applications. The electronic and magnetic properties of three organic–inorganic hybrid compounds with compositions $(NH_4)_2CuCl_4$, $(CH_3NH_3)_2CuCl_4$ and $(C_2H_5NH_3)_2CuCl_4$ are investigated for the first time with density functional theory plus on-site Coulomb interaction. A strong Coulomb interaction on the copper causes a relatively weak exchange coupling within the layers of the octahedral network, in good agreement with experiment. The character of the exchange interaction (responsible for magnetic behavior) is analyzed. The calculations reveal that $(C_2H_5NH_3)_2CuCl_4$ has the strongest Jahn–Teller (JT) distortion in comparison with the two other compounds. The easy axis of magnetization is investigated, showing a weak anisotropic interaction between inter-layer Cu^{2+} ions in the $(C_2H_5NH_3)_2CuCl_4$ structure. Orbital ordering is concluded from our partial density of states calculations: a cooperation of the JT distortion with an antiferro-distortive pattern.

(Some figures may appear in colour only in the online journal)

1. Introduction

Hybrid organic–inorganic compounds, synthesized by self-assembly from the solution, provide a considerable opportunity for scientific studies and technological applications [1–5]. This broad range of materials allows the combination of properties of organic and inorganic moieties within a single structure. The inorganic network can be considered as a collection of atoms that are held together by covalent and ionic interactions. The organic blocks, which generally interact through weaker interactions like hydrogen and van der Waals bonding, provide a degree of freedom to optimize magnetic and structural properties. Hybrid organic–inorganic compounds based on the perovskite structures are an interesting class of materials [4]. The basic building block of the organic–inorganic perovskite family is the ABX_3 perovskite structure. The structure consists of a 3D network of corner-sharing BX_6 octahedra in which the B atom is a metal cation, X is an anion, and A is selected as a cation in order to neutralize the total charge, and it can even be a molecule. In addition to the 3D perovskites, layered perovskite structures can be formed by slicing ABX_3 into slabs parallel to the [001] direction, with a thickness of one BX_6 octahedron. In this thought experiment the A and X atoms within the slice planes will be cut into halves. This situation can be improved by refilling the affected atoms, resulting in a structure of general formula A_2BX_4. The

term 'layered perovskite' has been chosen for this type of structure because one of the most characteristic features of perovskites is retained, i.e. the corner connection of BX_6 octahedra, although in two dimensions only [6, 7]. The structure comprises layers of corner-sharing BX_6 octahedra with the monovalent A cations occupying the cavities. The geometrical constraints parallel to the layers are similar to those of 3D perovskites, i.e. the positions of the A cations are laterally fixed in the holes of the network of the BX_6 octahedra. No constraint exists in the direction perpendicular to the layers. Individual layers can undergo distortion without interacting with neighboring layers, or layers can be shifted with respect to each other. The low-dimensional connectivity also enables development of low-dimensional magnetism [8]. Among the layered perovskite compounds the $(C_nH_{2n+1}NH_3)_2BCl_4$ in which $n = 0, 1, 2, \ldots$ have been studied experimentally in recent years [4, 5, 8–15] because of the promising magnetic and electronic properties. The $(C_nH_{2n+1}NH_3)^+$ groups fit well into the 2D pattern of the perovskite layers. The ammonium groups of the cations are connected to the halogens in the inorganic sheets by hydrogen bonds. The BCl_4^{2-} anions are thus sandwiched between organic sheets and the neutral layers formed stack onto each other [4, 15, 16]. The properties of the compounds with Cu differ from those with other transition metals [4, 8]. Firstly, divalent Cu^{2+} with the electronic configuration $3d^9$ ($t_{2g}{}^6e_g{}^3$) shows a substantial Jahn–Teller (JT) distortion. Hence, the strong JT effect gives rise to the distortion of octahedral coordination of the Cu^{2+} ion, with four short and two long bonds [17–19]. The elongated bonds of Cu–Cl on adjacent Cu^{2+} ions lie in the plane of the octahedral network and are oriented perpendicularly with respect to each other, forming an antiferro-orbital ordering [20]. Secondly, the JT effect yields different structural transitions in these compounds [11]. Thirdly, these materials show a range of 2D isotropic interaction that is offered by the Cu^{2+} compounds [8]. Fourthly, the ferromagnetic intra-layer interactions make them suitable for magnetic application in electronic devices. By contrast, the $M = Mn^{2+}$ and Fe^{2+} order antiferromagnetically [9].

Since the electronic structures of $(C_nH_{2n+1}NH_3)_2CuCl_4$ are not yet well known, we focus our attention on magnetic and electronic properties of three members of these materials for $n = 0$, 1 and 2 using density functional theory (DFT) plus on-site Coulomb interaction on Cu (DFT + U).

In this paper, the electronic structures of $(NH_4)_2CuCl_4$, $(CH_3NH_3)_2CuCl_4$ and $(C_2H_5NH_3)_2CuCl_4$ are presented: the appropriate structure (if needed) and electronic and magnetic properties are analyzed. Different magnetic configurations have been investigated in order to find the ground state. The calculations show a good agreement with experimental results. The magnetic interaction within the layers occurs via Cu–X…Cu chains in which X…Cu denotes the elongated copper chloride bond. Hence, the magnetic interaction is superexchange. In order to clarify the dominance of the superexchange interaction between metal ions within the layers, we consider the next-nearest-neighbor contributions. A comparison between the magnitude of the JT distortion is given. The compound that shows the strongest JT distortion is reported. Strong Coulomb interaction on the Cu is confirmed by comparing the estimated intra-layer exchange coupling constants for several U's with experiments. The influence of the on-site d–d Coulomb interaction on the band gap is shown. The partial density of states are plotted in order to see the existence of orbital ordering in a cooperation with JT distortion.

This paper is organized as follows. In section 2, we summarize the technical details of the calculations. The results concerning the structural, magnetic and electronic properties of these three organic–inorganic hybrids are discussed in sections 3 and 4. We analyze tilting of the octahedra, orbital ordering, JT effect and exchange coupling constants. We compare our results for these three compounds with experimental measurements (if data are available). Finally, in section 5 some conclusions are given.

2. Computational methods

Calculations were performed within the framework of density functional theory (DFT) [21, 22] and DFT plus on-site Coulomb interactions (DFT + U) [23] by using the PBE generalized gradient approximation (GGA) [24] and the projector augmented wave method (PAW) [25, 26] as implemented in the Vienna *Ab-initio* Simulation Package (VASP) [27, 28]. Since there are no unique data on the strength of the on-site Coulomb repulsion parameter U for Cu in the literature [29, 30], a known property of relevant materials is taken in order to find a suitable value of U (more details will be mentioned later). A fine Monkhorst–Pack grid of **k**-point has been chosen for sampling the Brillouin zone [31]. An energy cutoff of 400 eV has been used in all calculations. In order to see the effect of van der Waals interactions, we did a test run on one of the structures with an empirical correction for dispersion interactions added to the DFT, called DFT-D2 [32]. The calculations with van der Waals interactions have the same trend in underlying physical properties by comparison with standard DFT calculations; the effect of hydrogen bonding prevails for $n = 0$, 1 and 2. Spin–orbit interactions have been included in order to determine the direction of the easy axis. The atomic positions within the unit cell were relaxed until the forces were less than $F_{max} = 0.01$ eV Å^{-1}. The experimental data were used as a starting point for the optimization of atomic positions. Crystal structures were visualized by using the VESTA package [33].

3. The electronic properties of $(NH_4)_2CuCl_4$

The yellow compound $(NH_4)_2CuCl_4$ crystallizes in the orthorhombic cell with space group *Cmca* and lattice parameters $a = 15.46$ Å, $b = 7.20$ Å and $c = 7.20$ Å at room temperature [34]. (In order to be consistent with the two other compounds, we describe the structure of $(NH_4)_2CuCl_4$ with $a = 7.20$ Å, $b = 7.20$ Å and $c = 15.46$ Å as lattice parameters.) The structure is the first member of the $(C_nH_{2n+1}NH_3)_2CuCl_4$ compounds with square planar $CuCl_4^{2-}$ ions. The octahedral coordination of Cu^{2+} is

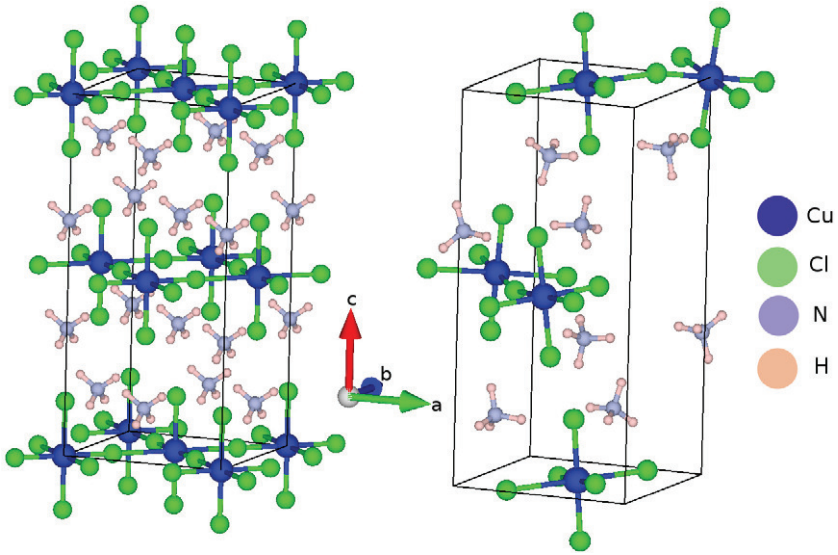

Figure 1. The initial (left) and optimized structure (right) of $(NH_4)_2CuCl_4$.

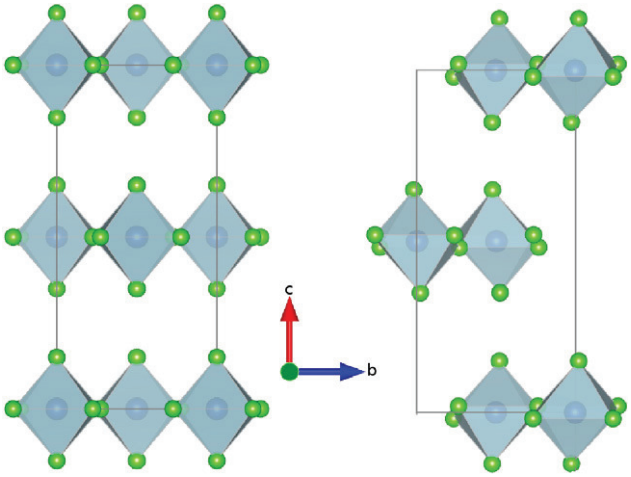

Figure 2. Tilting of the octahedra along the *c* axis. The untilted configuration (left) is compared with the tilted orthorhombic one (right).

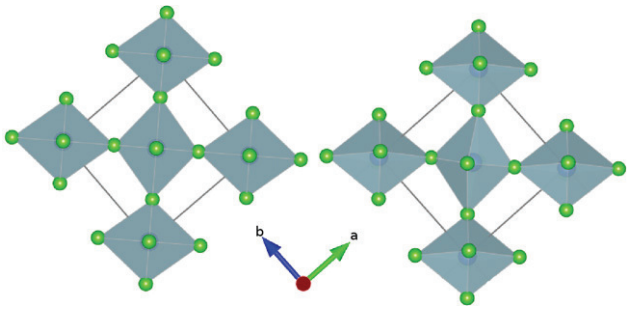

Figure 3. Tilting of $CuCl_6$ octahedral network in the *ab* plane; the untilted configuration (left) is compared with the tilted orthorhombic one (right).

completed by sharing two chlorine atoms from adjacent $CuCl_4^{2-}$ ions along one axis, as shown in figure 1. The Cu–Cl...Cu bond angle is linear (180°); no tilting with respect to the *c* axis or *ab* plane occurs (figures 2 and 3). The $(NH_4)^+$ groups occupy the holes between the chlorine atoms in the adjacent sheets. They form N–H···Cl bonds to any of the eight halogens, with four terminal and four bridging halogens. In order to find the ground state, we perform four calculations, nonmagnetic (N) and three different magnetic structures: ferromagnetic (FM), antiferromagnetic type 1 (ferromagnetic layers coupled antiferromagnetically, AFM_1) and antiferromagnetic type 2 (antiferromagnetic layers coupled antiferromagnetically, AFM_2) configurations. We used the x-ray diffraction data as the starting point for the optimization of the atomic positions. The initial positions of hydrogen atoms have been constructed, assuming a tetrahedral coordination for $(NH_4)^+$. The calculations reveal that the compound has a stable layer-type ferromagnetic structure, with a very weak antiferromagnetic interaction between the layers (AFM_1). A view of the optimized structure is shown in figure 1. The space group that results from our calculation, considering hydrogen atoms as well, has a lower symmetry. We determine *Pbca* as an appropriate space group for the optimized structure (table 1). The optimized Cu^{2+} lies approximately at the center of a distorted octahedron with two short (*s*) (2.28 Å), two long (*l*) equatorial (2.84 Å) and two medium (*m*) apical Cu–Cl (2.34 Å) bonds. The long equatorial Cu–Cl bond indicates a puckering of the $CuCl_4^{2-}$ sheets in the *ab* plane as a result of the hydrogen bonding interaction between the NH_4^+ groups and chloride ions. A schematic view of the perpendicular orientation of the neighboring long equatorial Cu–Cl bonds is shown in figure 4. A quantitative measure of the magnitude of the JT distortion is given by the octahedral distortion parameter (Δd) [35] defined as

$$\Delta d = (1/6) \sum_{1,6} [(d_n - d)/d]^2, \qquad (1)$$

in which d is the mean Cu–Cl bond distance and d_n are individual Cu–Cl bond distances. By mapping Cu–Cl distances onto equation (1), we have $\Delta d = 8.93 \times 10^{-3}$. The optimized octahedral network is tilted along the z axis

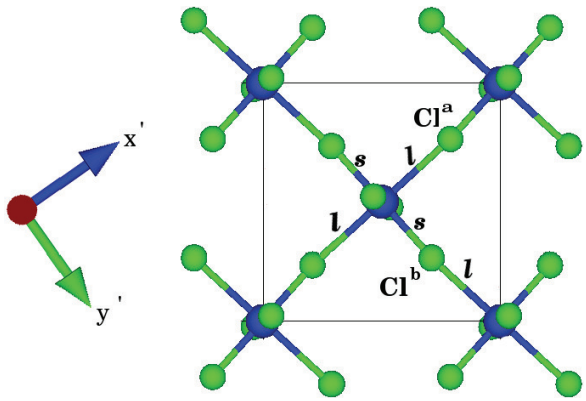

Figure 4. The schematic view of the alternation perpendicularly of the elongated Cu–Cl bonds in the *ab* plane. The Cl^a and Cl^b represent the interactions of p_x and p_y orbitals with the Cu atoms along x' and y' axes, respectively. The *s* and *l* stand for the short and long bonds, respectively. The unit cell is sketched for clarity.

Table 1. The position of atoms for the ground state of $(NH4)_2CuCl_4$ structure in the *Pbca* space group (no 61).

Atom	Wyckoff letter	*x*	*y*	*z*
Cu	4a	0.002	0.003	0.001
$Cl_1 \parallel ab$ plane	8c	0.208	0.232	0.019
$Cl_2 \perp ab$ plane	8c	0.034	0.020	0.150
N	8c	0.021	0.006	0.357
H_1	8c	0.015	0.358	0.124
H_2	8c	0.057	0.414	0.104
H_3	8c	0.018	0.490	0.207
H_4	8c	0.159	0.487	0.136

(figure 2). Each elongated Cu–Cl bond is slightly tilted from the [011] and [0$\bar{1}$1] directions (figure 3). The buckling angles of the octahedral network along the *ab* plane and *z* axis are $\theta_{ab} = 165.21°$ and $\theta_z = 5.60°$, respectively. The spin–orbit calculations show that the localized magnetic moments on each Cu lie in the *ab* plane ($E_{\perp_{ab}} - E_{\parallel_{ab}} = 1.0$ meV/Cu site). The density of states (DOS) and the projected density of states (PDOS) for different magnetic structures are shown in figures 5 and 6, respectively (consistently with figure 4). The partial density of states in figure 6 indicates that the d states of Cu interact indirectly through the states of Cl. Since the unoccupied Cu d states are not noticeably narrower in the case of antiferromagnetic alignment, the direct interaction of Cu atoms is not significant (figure 6). The band gap is predominantly by e_g orbitals of the Cu d states: compare figure 5 with figure 6. The perpendicularity of the elongated Cu–Cl octahedra bonds in the *ab* plane give rises to the alternating arrangement of $d_{z^2-x^2}$ and $d_{z^2-y^2}$ [36, 37]. This alternation of $d_{z^2-x^2}$ and $d_{z^2-y^2}$ as a result of the two possible combinations of the $d_{z^2-r^2}$ and $d_{x^2-y^2}$ atomic orbitals can be derived from the alternating favorable interaction of Cl p_x and p_y with e_g states (figure 7).

The order of magnitude and sign of the exchange interaction can be estimated by the Heisenberg model [38].

$$H = -\sum_{i,j} J_{ij}\mathbf{S_i} \cdot \mathbf{S_j}. \qquad (2)$$

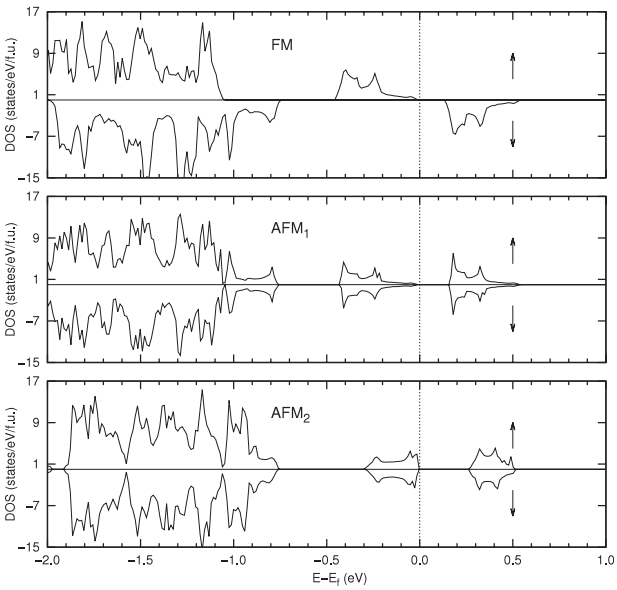

Figure 5. Total density of states for FM, AFM_1 and AFM_2 configurations of $(NH_4)_2CuCl_4$ structure with $U = 0$ eV.

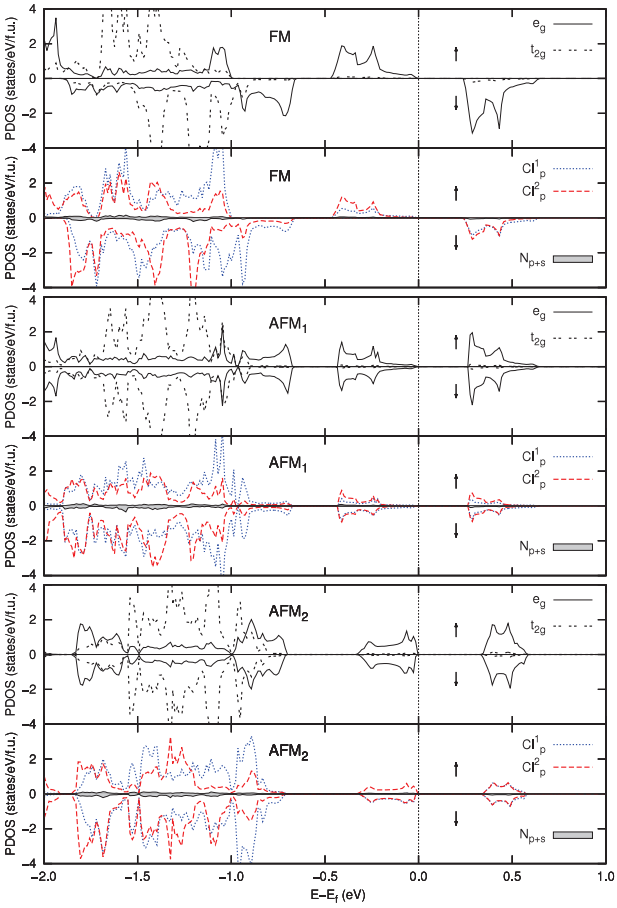

Figure 6. PDOS of Cu d, Cl_p^1, Cl_p^2 and N_{p+s} (p + s orbitals of N) for FM, AFM_1 and AFM_2 configurations of $(NH_4)_2CuCl_4$ structure with $U = 0$ eV.

The summation is taken over the neighboring spins; J_{ij} denotes the exchange constant between spins and **S** is the operator magnetic moment on each copper. The character of

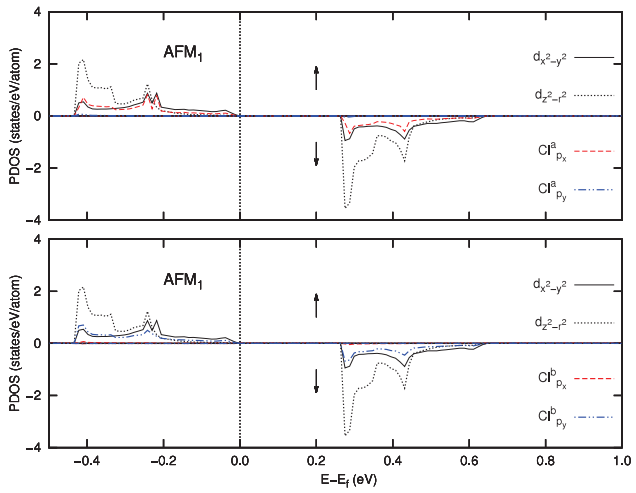

Figure 7. The PDOS of the alternating interaction of Cl p states (p orbitals in the *ab* plane) with e_g states of Cu within the layers of octahedra (*ab* plane) for AFM_1 alignment of $(NH_4)_2CuCl_4$ structure with $U = 0$ eV.

Table 2. The calculated J/k_B and the experimental measurement (exp.) [8] (in K) for $(NH_4)_2CuCl_4$ structure from GGA and GGA + U calculations.

	Exp.	$U = 0$ eV	$U = 7$ eV
J/k_B	17	80.0	19

the exchange interaction in our compounds (predominantly a weak intra-layer interaction) is superexchange, as a result of short range interactions. In order to check the dominance of the superexchange interaction, we expand our cell in the *ab* plane. We double the tetragonal unit cell by rotation of 45° and lattice parameters; $c' = c$ and $a' = b' = a\sqrt{2}$. This supercell is chosen in order to realize different types of magnetic ordering within the same unit cell. The values for the nearest-neighbor (NN) and next-nearest-neighbor (NNN) intra-layer interactions show a weaker contribution of the NNN interaction (by one order of magnitude). Hence, there is a dominance of the superexchange interaction. This short range of the superexchange interaction here is the reason for the loss of a significant part of the interaction between neighbors along the longest (z) direction. We express the energy (equation (2)) for FM and AFM_2 configurations in terms of the nearest-neighbor interaction within the layers, J. A comparison between the theoretically calculated, J_{cal}, and experimentally [8] determined exchange constant, J_{exp}, is given in table 2. The difference between the experimental and theoretical intra-layer exchange coupling constants is a result of electron correlation on the Cu atom. The electron correlation associated with the Cu 3d state was taken into consideration by performing GGA plus on-site Coulomb repulsion (GGA + U) calculations. We investigated the relative energies of the FM and AFM_1 type of spin ordering from our GGA + U calculations written in terms of a Heisenberg exchange Hamiltonian, equation (2). The variation in the superexchange constant within the layers J (in K) as a function of U (in eV) is depicted in figure 8.

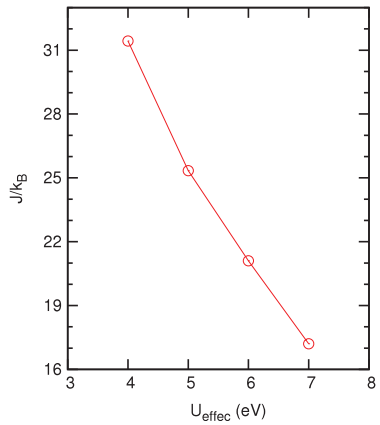

Figure 8. The variation in intra-layer exchange coupling constants J/k_B (in K) with U (in eV) for the $(NH_4)_2CuCl_4$ structure.

The comparison of the intra-layer exchange coupling constant in GGA + U calculations with the experimental one gives rise to a suitable value of $U = 7$ eV, given in table 2. The atomic positions with $U = 7$ eV are almost the same (with a maximum difference of (0.0032, 0.0037, 0.0014 Å) between them). In this calculation ($U = 7$ eV), we have $\theta_{ab} = 165.14°$, $\theta_z = 7.72°$, and the magnitude of the JT distortion, $\Delta d = 1.37 \times 10^{-2}$ (equation (1)). The DOS and PDOS (for Cu d and Cl p states) with $U = 7$ eV are shown in figure 9.

4. The electronic properties of $(CH_3NH_3)_2CuCl_4$

The monoclinic structure of $(CH_3NH_3)_2CuCl_4$ (space group $P2_1/a$ and lattice parameters $a = 7.155$ Å, $b = 7.424$ Å, $c = 9.814$ Å and $\beta = 109.18°$ at $T = 100$ K) shows the JT distorted octahedron [16, 39, 40]. The compound is a second example of square planar $CuCl_4^{2-}$ ions from $(C_nH_{2n+1}NH_3)_2CuCl_4$ perovskite structures, as is shown in figure 10. The methylammonium moieties are located between the layers and connected by hydrogen bonds to the Cl^- ions, leading to one bridging and two terminal chlorine ligands. In order to find the ground state, we construct a monoclinic unit cell with the same a and b parameters and c twice the primitive lattice parameter. We consider five calculations, nonmagnetic (N) and four different magnetic structures: ferromagnetic (FM) and antiferromagnetic type 1 (AFM_1), antiferromagnetic type 2 (AFM_2) and antiferromagnetic type 3 (AFM_3) configurations, based on the number of the nearest-neighbors and the sign of the superexchange interaction (figure 11). The compound favors an isolated two-dimensional ferromagnetic alignment (negligible energy difference between FM and AFM_1 structures). The Cu^{2+} has distorted octahedral coordinates, with two short (s) (2.29 Å), two medium (m) (2.33 Å) and two long (l) (2.91 Å) Cu–Cl bonds. The elongated Cu–Cl bonds are orientated perpendicularly to each other (figure 12). By using equation (1), we have the magnitude of the JT distortion, $\Delta d = 1.12 \times 10^{-2}$. The structure is tilted along the z axis ($\theta_z = 9.11°$) and the *ab* plane ($\theta_{ab} = 163.51°$). The

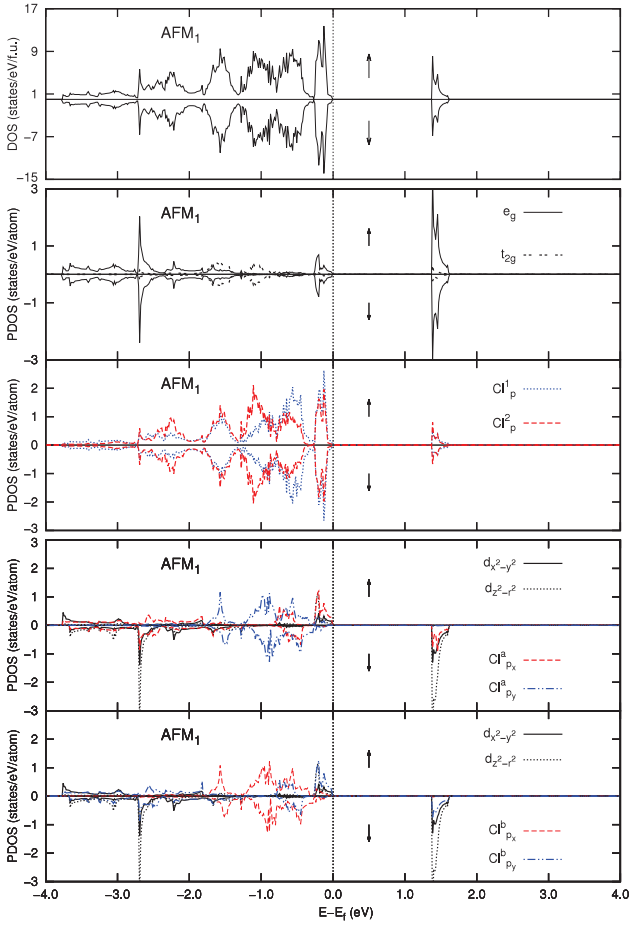

Figure 9. The DOS, PDOS and alternating interaction of Cl p states (p orbitals in the *ab* plane) with e_g states of Cu within the layers of octahedra (*ab* plane) with $U = 7$ eV, for AFM_1 alignment of $(NH_4)_2CuCl_4$ structure (note the different energy scale compared to DOS and PDOS plots with $U = 0$ eV).

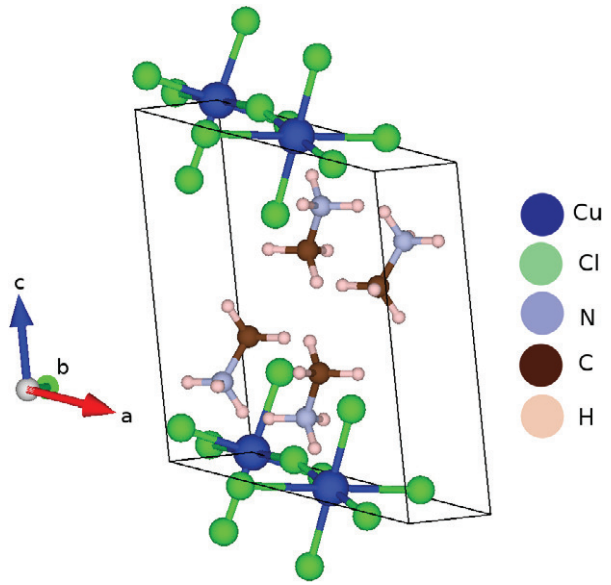

Figure 10. The structure of $(CH_3NH_3)_2CuCl_4$; the octahedra are sandwiched between methylammonium groups.

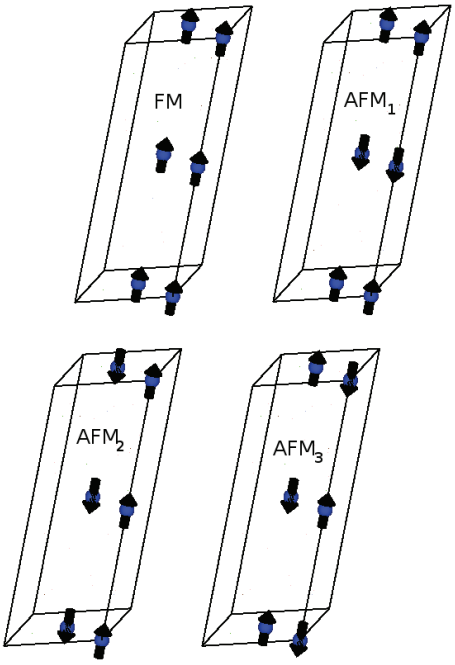

Figure 11. The schematic depiction of FM, AFM_1, AFM_2 and AFM_3 configurations. The arrows on each Cu represent spin direction.

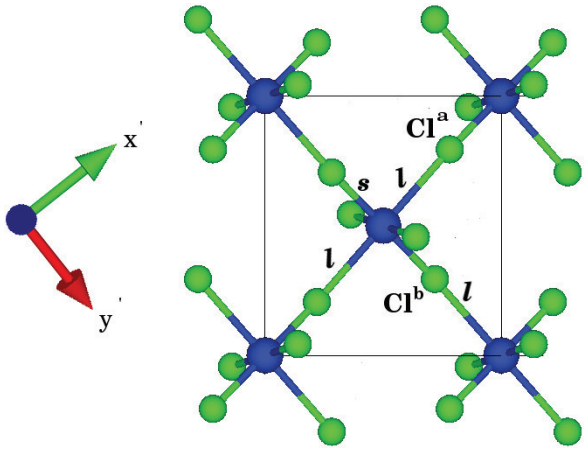

Figure 12. A schematic view of the antiferro-orbital ordering in the *ab* plane. The Cl^a and Cl^b represent the interaction of p_x and p_y with the Cu atoms along x' and y' axes, respectively. The *s* and *l* stand for the short and long bonds, respectively. The unit cell is sketched for clarity.

tilting of the octahedral network in the *ab* plane and along the *c* axis is depicted in figure 13. The C–N groups are almost perpendicular to the *ab* plane with angles of $\theta_a = 79.64°$ and $\theta_b = 67.92°$ with respect to the *a* and *b* axes, respectively. The size of the intra-layer exchange coupling constant, by using equation (2) and considering the relative energy of the ferromagnetic and antiferromagnetic alignment, is given in table 3. The difference in magnetic anisotropy shows that the localized magnetic moments on each Cu atom lie in the *ab* plane ($E_{\|_c} - E_{\|_{ab}} = 1.0$ meV/Cu site). The density of states (DOS) and projected density of states (PDOS) for

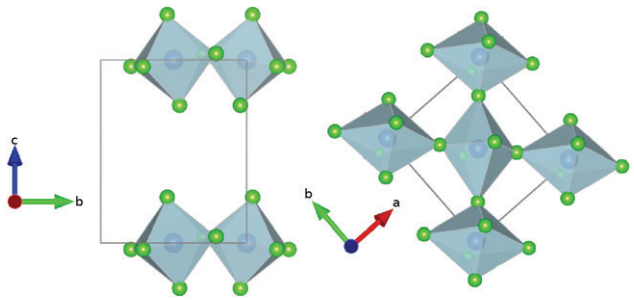

Figure 13. A tilted perspective of $(CH_3NH_3)_2CuCl_4$ in the *ab* plane and along the *c* axis. The unit cell is sketched for clarity.

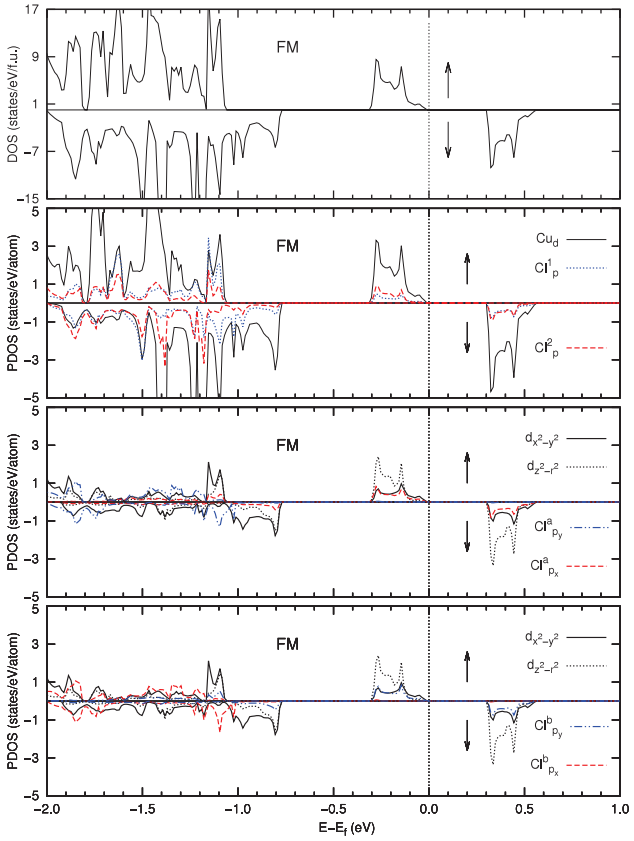

Figure 14. The DOS and PDOS for ferromagnetic (FM) configuration of $(CH_3NH_3)_2CuCl_4$ with $U = 0$ eV.

Cu d and Cl p orbitals of the ground state are shown in figure 14 (consistently with figure 12). A comparison between DOS and PDOS confirms the dominance of the Cu d orbital around the band gap. The appearance of elongated distorted octahedra [36, 37] gives rise to the alternation of $d_{z^2-x^2}$ and $d_{z^2-y^2}$ type orbitals, as a result of cooperative JT distortion with ferromagnetic ordering of $CuCl_6$ octahedra (figure 14). Now, we express the relative energy of the ferromagnetic and antiferromagnetic configurations, by using equation (2), from DFT + U with $U = 7$ eV in order to estimate the intra-layer exchange coupling constant. In this calculation, the size of the exchange coupling parameter is given in table 3; also, we have $\theta_{ab} = 163.16°$, $\theta_z = 9.23°$ and $\Delta d = 1.49 \times 10^{-2}$.

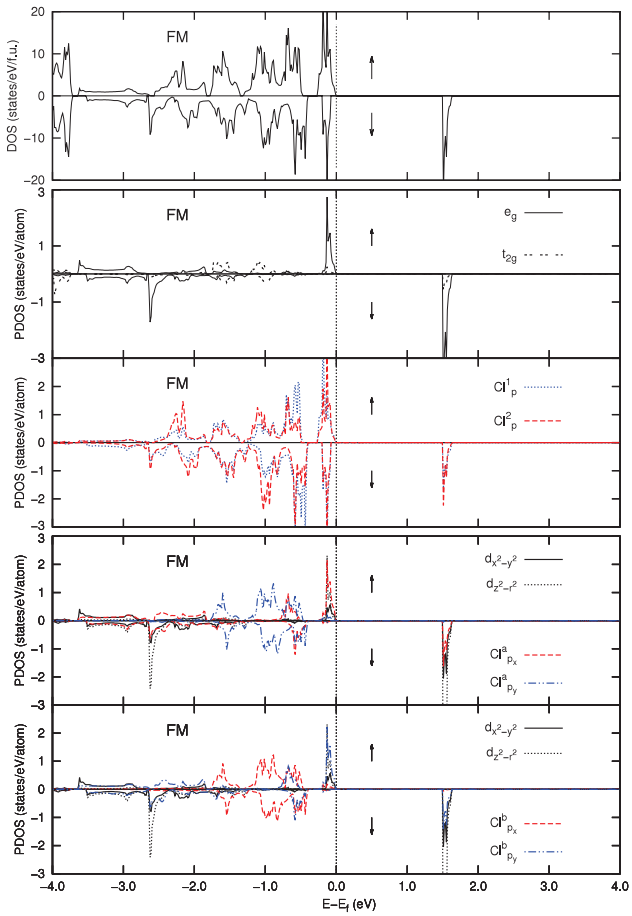

Figure 15. The DOS and PDOS for ferromagnetic (FM) configuration of $(CH_3NH_3)_2CuCl_4$ with $U = 7$ eV (note the different energy scale compared to figure 14).

Table 3. The estimated J/k_B and the experimental measurement (exp.) [8] (in K) for the $(CH_3NH_3)_2CuCl_4$ compound from GGA and GGA + U calculations with $U = 7$ eV.

	Exp.	$U = 0$ eV	$U = 7$ eV
J/k_B	19.2	82.2	21

The DOS and PDOS (for Cu d and Cl p orbitals) with $U = 7$ eV are shown in figure 15. The calculated parameter, J, from GGA + U calculation shows a good agreement with experimental measurement [8].

5. The electronic properties of $(C_2H_5NH_3)_2CuCl_4$

The compound $(C_2H_5NH_3)_2CuCl_4$ [15, 18, 19] is the third member of the $(C_nH_{2n+1}NH_3)_2CuCl_4$ series with the square planar $CuCl_4^{-2}$. The lattice constants of $(C_2H_5NH_3)_2CuCl_4$ are $a = 7.47$ Å, $b = 7.17$ Å and $c = 21.24$ Å at $T = 100$ K with the *Pbca* space group [41]. The face-centered orthorhombic unit cell is shown in figure 16. We construct four calculations, nonmagnetic (N) and three different magnetic orderings: including ferromagnetic (FM), antiferromagnetic type 1 (ferromagnetic layers coupled antiferromagnetically

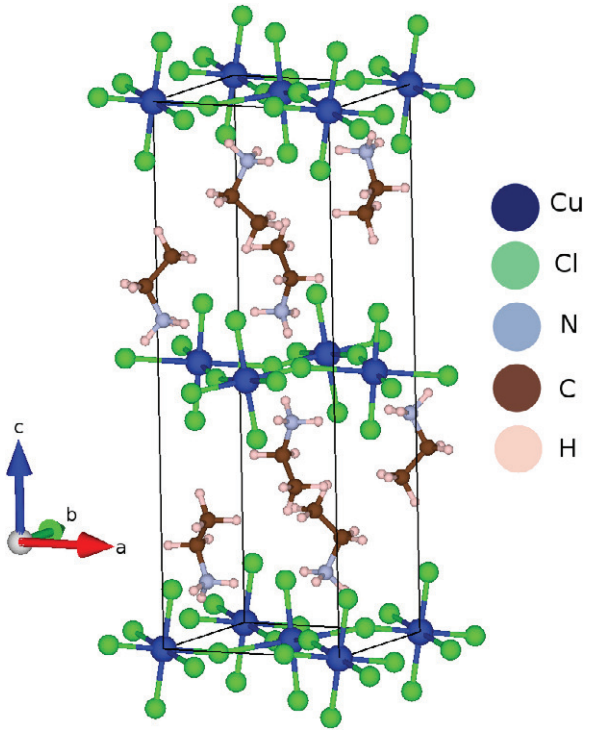

Figure 16. The structure of $(C_2H_5NH_3)_2CuCl_4$; the $CuCl_6$ sheets are sandwiched between two layers of ethylammonium.

Table 4. The estimated J/k_B and the experimental measurement (exp.) [8] (in K) for the $(C_2H_5NH_3)_2CuCl_4$ compound from GGA and GGA + U calculations with $U = 7$ eV.

	Exp.	$U = 0$ eV	$U = 7$ eV
J/k_B	18.6	83	20

AFM_1) and antiferromagnetic type 2 (antiferromagnetic layers coupled antiferromagnetically AFM_2) in order to find the ground state. The compound favors a layered-ferromagnetic structure with a very weak antiferromagnetic coupling between the layers. The Cu^{2+} ions are located approximately in the center of a distorted octahedron with two short (s) (2.29 Å), two medium (m) (2.32 Å) and two long (l) (2.93 Å) Cu–Cl bonds. The alternate elongated Cu–Cl bonds are perpendicular to each other (figure 17). The magnitude of the JT distortion, by using equation (1), is $\Delta d = 1.21 \times 10^{-2}$. The octahedral network is tilted with respect to the ab plane and the z axis with angles of $\theta_{ab} = 163.75°$ and $\theta_z = 8.95°$, respectively. The neighboring octahedra along the ab plane and the z axis have the same tilting direction. The size of intra-layer exchange coupling constant, by mapping the relative energy of FM and AFM_1 alignment onto the Heisenberg model (equation (2)), is given in table 4. The calculated energy difference ($E_{\perp_{ab}} - E_{\parallel_{ab}} = 0.90$ meV/Cu site) implies that the magnetic moments on copper atoms lie in the ab plane with a very small deviation in comparison with two former structures. The density of states (DOS) and projected density of states (PDOS) of the structure for the ground state is shown in figure 18 (consistently with

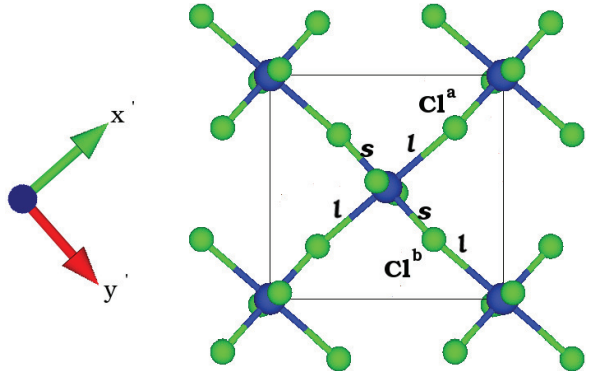

Figure 17. A schematic view of the antiferro-orbital ordering in the ab plane. Cl^a and Cl^b represent the interaction of p_x and p_y with the Cu atoms along x' and y' axes, respectively. s and l stand for the short and long bonds, respectively. The unit cell is sketched for clarity.

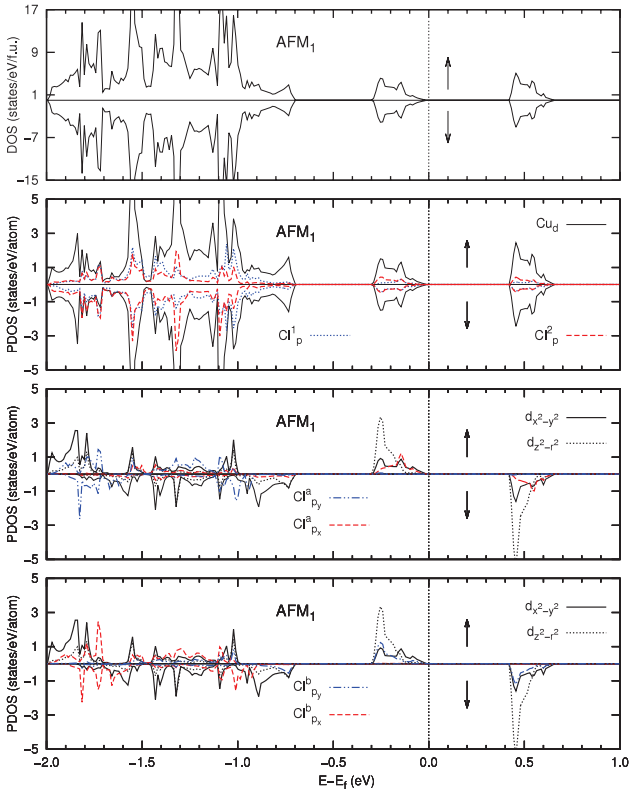

Figure 18. The DOS and PDOS for antiferromagnetic type 1 (AFM_1) $(C_2H_5NH_3)_2CuCl_4$ with $U = 0$ eV.

figure 17). The band gap is mostly dominated by Cu d orbitals, and the alternating arrangement of $d_{z^2-x^2}$ and $d_{z^2-y^2}$ orbitals is confirmed from the PDOS in figure 18, as a result of cooperative JT distortion with antiferro-orbital ordering of $CuCl_6$ octahedra. The intra-layer exchange parameter from DFT + U with $U = 7$ eV is given in table 4, in good agreement with experiment. For $U = 7$ eV we have $\theta_{ab} = 163.45°$, $\theta_z = 9.12°$ and $\Delta d = 1.70 \times 10^{-2}$. Also the DOS and PDOS (for Cu d and Cl p orbitals) are shown in figure 19.

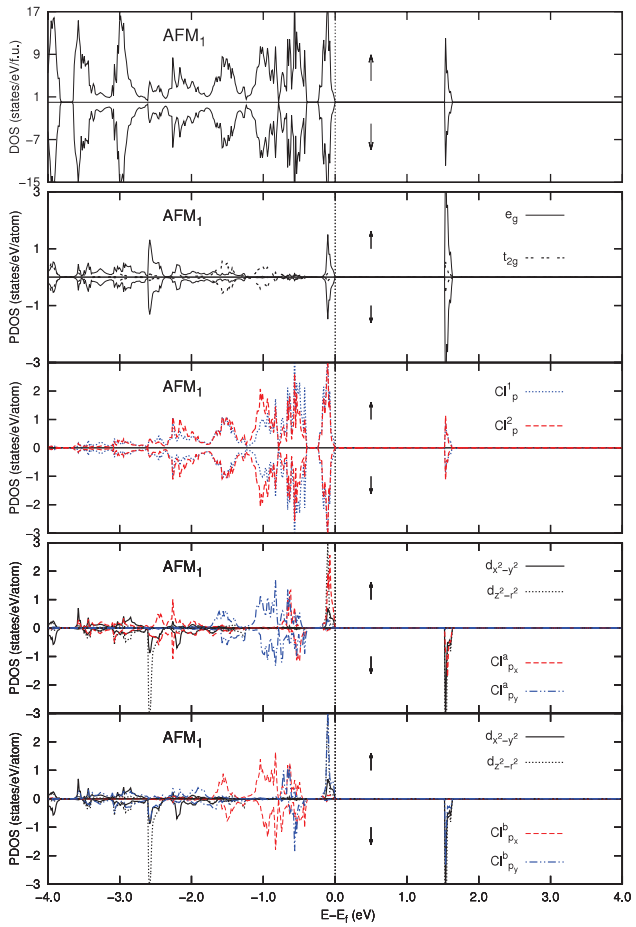

Figure 19. The DOS and PDOS for antiferromagnetic type 1 (AFM_1) $(C_2H_5NH_3)_2CuCl_4$ with $U = 7$ eV (note the different energy scale compared with figure 18).

6. Conclusion

We have given a detailed analysis of the electronic properties of the three organic–inorganic hybrids with formulas $(NH_4)_2CuCl_4$, $(CH_3NH_3)_2CuCl_4$ and $(C_2H_5NH_3)_2CuCl_4$. A weak contribution of the next-nearest-neighbor interaction (one order of magnitude smaller than the nearest-neighbor interaction) results in the dominance of the superexchange interaction within the layers. With GGA + U ($U = 7$ eV) good agreement with the experimental intra-layer exchange coupling constant is obtained. The Jahn–Teller effect is stronger for the compound with the longest organic cation, $(C_2H_5NH_3)_2CuCl_4$, in DFT and DFT + U calculations. In fact, we found a linear relation between the magnitude of the Jahn–Teller distortion and the length of the organic cation. The anisotropic interaction between Cu^{2+} ions in $(C_2H_5NH_3)_2CuCl_4$ is stronger than in the two other compounds, in spite of the increasing length of one (z) direction as a result of the increasing organic cation sizes. The relatively appreciable anisotropy for $(C_2H_5NH_3)_2CuCl_4$ may be a result of the appreciable effect of magnetic dipolar interactions (of the order of 10^{-4} in K) as well as superexchange interactions between the layers. The existence of orbital ordering is shown from our partial density of states (PDOS) calculations as a result of the alternating interaction of the two possible combinations of $d_{z^2-x^2}$ and $d_{z^2-x^2}$ orbitals with Cl p_x and Cl p_y orbitals. We show that the contributions of the inorganic components, by considering the antiferro-distortive pattern of the octahedral network and the manner of orbital ordering, are similar in these three compounds. The organic contributions, however, vary significantly for different organic components. It is interesting to mention that the octahedral tilting has been modified with respect to the temperature as well as the organic constituent: the absence of the tilting for the $(NH_4)_2CuCl_4$, $\theta_{ab} = 170.96°$ for the $(CH_3NH_3)_2CuCl_4$, and $\theta_{ab} = 169.63°$ for the $(C_2H_5NH_3)_2CuCl_4$ at room temperature are the evidence for this effect.

Acknowledgments

This work was carried out with the support of the Stichting voor Fundamenteel Onderzoek der Materie (FOM). FOM is financially supported by the Nederlandse Organisatie voor Wetenschappelijk Onderzoek (NWO).

References

[1] Sanchez C, Julian B, Belleville P and Popall M 2005 *J. Mater. Chem.* **15** 3559
[2] Gomez-Romero P 2001 *J. Adv. Mater.* **13** 163
[3] Mammeri F, Le Bourhis E, Rozes L and Sanchez C 2005 *J. Mater. Chem.* **15** 3787
[4] Mitzi D B 1999 *Prog. Inorg. Chem.* **48** 1 (and refrences therein)
[5] Rao C N R, Cheetham A K and Thirumurugan A 2008 *J. Phys.: Condens. Matter* **20** 159801
[6] Heger G, Mullen D and Knorr K 1975 *Acta Crystallogr.* A **31** S189
[7] Haegele R and Babel D 1974 *Z. Anorg. Allg. Chem.* **409** 11
[8] de Jongh L J and Miedema A R 1978 *J. Appl. Phys.* **49** 1305
[9] Mikhail I 1977 *Acta Crystallogr.* B **33** 1317
[10] Willett R D 1990 *Acta Crystallogr.* C **46** 565
[11] Tello M J, Manes J L, Fernandez J, Arriandiaga M A and Perezmato J M 1981 *J. Phys. C: Solid State Phys.* **14** 805
[12] Dupas A, Ledang K, Renard J P and Veillet P 1977 *J. Phys. C: Solid State Phys.* **10** 3399
[13] Willett R D and Riedel E F 1975 *Chem. Phys.* **8** 112
[14] Vanamste W D and de Jongh L J 1972 *Solid State Commun.* **11** 1423–9
[15] de Jongh L J, Vanamste W D and Miedema A R 1972 *Physica* **58** 277
[16] Pabst I, Fuess H and Bats J W 1987 *Acta Crystallogr.* C **43** 413
[17] Barendre F and Schenk H 1970 *Physica* **49** 465
[18] Steadman J P and Willett R D 1970 *Inorg. Chim. Acta* **4** 361
[19] Jahn I R, Knorr K and Ihringer J 1989 *J. Phys.: Condens. Matter* **1** 6005
[20] Khomskii D I 2005 *Phys. Scr.* **72** CC8
[21] Hohenberg P and Kohn W 1964 *Phys. Rev.* **136** B864
[22] Kohn W and Sham L J 1965 *Phys. Rev.* **140** A1133
[23] Liechtenstein A I, Anisimov V I and Zaanen J 1995 *Phys. Rev.* B **52** R5467
[24] Perdew J P, Burke K and Ernzerhof M 1996 *Phys. Rev. Lett.* **77** 3865
[25] Blöchl P E 1994 *Phys. Rev.* B **50** 17953
[26] Kresse G and Joubert D 1999 *Phys. Rev.* B **59** 1758
[27] Kresse G and Furthmüller J 1996 *Phys. Rev.* B **54** 11169
[28] Kresse G and Furthmüller J 1996 *Comput. Mater. Sci.* **6** 15

[29] Anisimov V I, Korotin M A, Nekrasov I A, Pchelkina Z V and Sorella S 2002 *Phys. Rev.* B **66** 100502
[30] Laskowski R, Blaha P and Schwarz K 2003 *Phys. Rev.* B **67** 075102
[31] Monkhorst H J and Pack J D 1976 *Phys. Rev.* B **13** 5188
[32] Grimme S 2006 *J. Comput. Chem.* **27** 1787
[33] Momma K and Izumind F 2008 *J. Appl. Crystallogr.* **41** 6523
[34] Willett R D 1964 *J. Chem. Phys.* **41** 2243
[35] Alonso J A, Martinez-Lope M J, Casais M T and Fernandenz-Diaz M T 2000 *Inorg. Chem.* **39** 917
[36] Khomskii D I and Kugel K I 1973 *Solid State Commun.* **13** 763
[37] Khomskii D I and Kugel K I 1982 *Usp. Fiz. Nauk* **136** 621
[38] Ashcroft N W and Mermin N D 1976 *Solid State Physics* (Stamford, CT: Cengage Learning)
[39] Steijger J J M, Frikkee E, de Jongh L J and Huiskamp W J 1988 *Physica* B+C **123** 284
[40] Steijger J J M, Frikkee E, de Jongh L J and Huiskamp W J 1984 *Physica* B+C **123** 271
[41] Polyakov A O 2011 private communication